Special Issue: This submission is for the Igor Sevostianov Memorial Issue

MMS

Mathematics and Mechanics of Solids
1–15

DOI: 10.1177/10812865221108373
journals.sagepub.com/home/mms
SAGE

Resistivity contribution tensor for two non-conductive overlapping spheres having different radii[AQ: 1]

[AQ1]: Article title is correct

Luca Lanzoni
Dipartimento di Ingegneria "Enzo Ferrari," Università di Modena e Reggio Emilia, Modena, Italy

Enrico Radi
Dipartimento di Scienze e Metodi dell'Ingegneria, Università di Modena e Reggio Emilia, Reggio Emilia, Italy

Igor Sevostianov
Department of Mechanical and Aerospace Engineering, New Mexico State University, Las Cruces, NM, USA

Received 21 December 2021; accepted 3 June 2022

Abstract
We consider here the problem of a three-dimensional (3D) body subjected to an arbitrarily oriented and remotely applied stationary heat flux. The body includes a non-conductive inhomogeneity (or pore) having the shape of two intersecting spheres with different radii. Using toroidal coordinates, the steady-state temperature field and the heat flux have been expressed in terms of Mehler–Fock transforms. Then, by imposing Neumann BCs at the surface of the spheres, a system of two Fredholm integral equations is obtained and solved based on Gauss–Laguerre quadrature rule. It is shown that the components of the resistivity contribution tensor exhibit a non-monotonic trend with the distance between sphere centers. In particular, if the inhomogeneity has a symmetric dumbbell-shape, then the extrema of the resistivity contribution tensor components occur when the two overlapping spheres have the same size. Differently, when the inhomogeneity has a lenticular shape, then these extrema are attained for a non-symmetric configuration, namely, for different radii of the intersecting spheres.

Keywords
Overlapping spheres, steady-state temperature field, resistivity contribution tensor, Mehler–Fock transforms, toroidal coordinates

Corresponding author:
Luca Lanzoni, Dipartimento di Ingegneria "Enzo Ferrari," Università di Modena e Reggio Emilia, Via Vivarelli, 10, 41125 Modena, Italy.
Email: luca.lanzoni@unimo.it

1. Introduction

Many experimental studies in the framework of advanced materials science recently showed the potential of realizing smart composites embedding pores or inhomogeneities of special shape. Indeed, physical and chemical properties of microstructured materials are highly affected by the form of the inhomogeneities embedded in the background matrix. Therefore, the size and shape of the inclusions can be properly designed with the aim to give smart materials with specific performances. As an example, Park et al. [1] displayed a method of synthesizing dumbbell-shaped polymer nanoparticles with dimensions of some hundred nanometers and large aspect ratios to obtain photonic materials with specific optical properties. In such a study, particles having the shape of a pair of overlapping spheres can be obtained starting from core-shell spherical particles, as shown in Figure 1 [2]. Under proper polymerization conditions, an additional lobe forms and grows on the surface of the nanoparticle, thus giving rise to a dumbbell-shaped particle (e.g., [3–7]). This phenomenon allows realizing three-dimensional (3D) photonic crystals, which deserved a lot of interest in the last decade as they exhibit band gap formation during electromagnetic wave propagation. This occurrence leads to the realization of a variety of high-tech disposals like filters, mirrorless lasers, and other smart devices with tunable electromagnetic properties [8]. As shown by Velikov [9], non-spherical particles can also be obtained by exploiting ion irradiation applied to monodisperse silica nanoparticles of spherical shape to obtain oblate or prolate ellipsoids. Moreover, dispersed dumbbell particles exhibit nematic phase behavior, which is the working principle of liquid crystals based on colloidal particles [10].

Dumbbell-shaped inhomogeneities can also take place due to coalescence and growth of spherical pores during synthesis and manufacturing processes of various materials, with special reference to metal alloys, sintered ceramics, sprayed coatings, foamed metals, and so on. As an example, the pore coalescence induced by specific heat treatments in foamed titanium has been investigated by Shen et al. [11]. Based on metallographic observations, simulations of the 3D microstructure are developed in that work to reproduce the evolution of the microstructure during foaming, thus allowing realizing predictive finite element (FE) analyses.

A homogenization scheme to assess the effective elastic properties of sintered porous materials including merging spherical pores has been addressed in Manoylov et al. [12] based on a statistical approach. Various distribution functions of merging pores are considered in that study to predict the elastic moduli of sintered synthetic sandstone and various metallic foams varying the total porosity. However, it is remarked that merged spherical pores have been simulated by considering prolate spheroids of the same volume, thus approximating the real shape of the voids. This preliminary attempt confirms that an accurate investigation of the properties of microstructured materials including inhomogeneities of non-ellipsoidal shape has not been well developed. However, the (quite usual) approximation of inhomogeneities of various shapes as "equivalent" ellipsoids of identical aspect ratio and/or equal volume can lead to rough predictions [13]. Moreover, Forster et al. [2] found that polymer dumbbell nanoparticles can self-assemble into a dense crystalline packing having a packing fraction higher than the densest

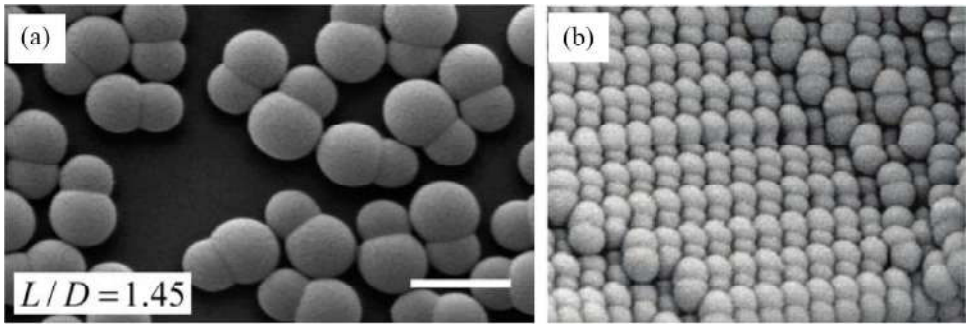

Figure 1. (a) Dumbbells synthesized starting from spherical core-shell nanoparticles through seeded emulsion polymerization (from Park et al. [1]). (b) SEM image of a crystal structure formed by polymer dumbbells in an aqueous suspension and self-assembled through an external electric field (from Forster et al. [2]).
L/*D* stands for the length/diameter ratio, whereas the white bar represents 0.5 μm.

known packings of spheres and ellipsoids. In this case, the approximation by ellipsoidal shape usually adopted for calculating the effective properties of clusters of particles having irregular shape does not provide correct results for this kind of inhomogeneities, which require instead an appropriate procedure. For these motivations, accurate investigations were already performed to define the effective conductive properties of composites containing inhomogeneities of complex shapes [14–16]. In particular, the components of the resistivity contribution tensor of such inhomogeneities were calculated analytically and then compared with the predictions obtained for equivalent spheroids. Later, the study was also extended to assess the effective elastic properties of composites containing inhomogeneities of complex shapes [17,18].

The present work lays within this direction. It addresses indeed the thermal conductivity problem of a 3D isotropic medium enclosing an insulating inhomogeneity having the shape of two overlapping spheres of different size. This allows assessing the effective thermal conductivity of a wide range of materials. It is worth noticing that the same approach can be performed to evaluate other physical properties, like the overall electric conductivity and the effective diffusivity in non-homogeneous media involving such kind of inhomogeneity.

The system considered here is subjected to a stationary, remotely applied and arbitrarily oriented heat flux. The solution in terms of temperature field is sought as the sum of two contributes: the first one is the temperature field related to a homogeneous medium, whereas the second one denotes the corrective term that allows satisfying the Neumann boundary condition at the surface of the insulated inhomogeneity. Based on the geometrical layout, reference is made to toroidal coordinates. The unknown temperature field satisfying the Laplace equation in then expressed in terms of Mehler–Fock transforms involving the Legendre functions. This formalism allows obtaining an analytical expression of the solution in the transformed domain as a convergent integral of two unknown functions. The fulfillment of the BCs leads to a system of two independent Fredholm integral equations, which is solved numerically by applying the Gauss–Laguerre quadrature rule. The aforementioned procedure is employed both for the problems of a remotely applied heat flux directed along the axis of symmetry of the inhomogeneity (axisymmetric problem) and a heat flux applied orthogonal to it. The components of the resistivity contribution tensor are finally assessed as surface integrals involving the temperature distributions on the spheres calculated for the two basic cases. The study generalizes the results reported in Lanzoni et al. [16] for the case of media embedding two overlapping spherical pores of equal size.

The paper is organized as follows. The formulation of the problem is reported in section 2. In particular, the problem of a heat flux directed along the symmetry axis is handled in section 3, whereas a heat flux applied orthogonally to the symmetry axis is addressed in section 4. The components of the resistivity contribution tensor are assessed in section 5, together with a comparison with the analytical predictions obtained for equivalent spheroids. Finally, conclusions are drawn in section 6.

The results obtained here allow evaluating the overall conductivity properties of materials with microstructures involving non-conductive inhomogeneities resembling dumbbell-shaped according to the usual homogenization schemes (e.g., non-interaction approximation, self-consistent scheme, and *Maxwell* scheme).

2. Formulation of the problem in toroidal coordinates

Let us consider a pore formed by two intersecting spheres of different sizes (see Figure 2). The sphere in the upper part of the xy-plane has radius R_1 and is centered at the point $(0, 0, z_1)$, whereas the sphere in the lower part has radius R_2 and is centered at $(0, 0, z_2)$. An insulated inhomogeneity embedded in an infinite conductive homogeneous medium subject to a stationary remotely applied heat flux is considered here. Accordingly, the boundary condition on the pore surface requires the vanishing of the normal component of the heat flux. Following Morse and Feshbach [19] and Lebedev et al. [20], we introduce a toroidal coordinate system (α, β, γ) defined by the following relations:[AQ: 2][AQ: 3]

[AQ2]: equations have been renumbered properly and corectly quoted within the main text

$$x = \frac{a \sinh\alpha \cos\gamma}{\cosh\alpha - \cos\beta}, \quad y = \frac{a \sinh\alpha \sin\gamma}{\cosh\alpha - \cos\beta}, \quad z = \frac{a \sin\beta}{\cosh\alpha - \cos\beta}. \tag{1}$$

where a denotes the distance of the poles from the origin, $a > 0$, $\alpha \in [0, \infty)$, $\beta \in [-\pi, \pi)$, and $\gamma \in [0, 2\pi)$.

[AQ3]: Greek symbols and other variables are ok

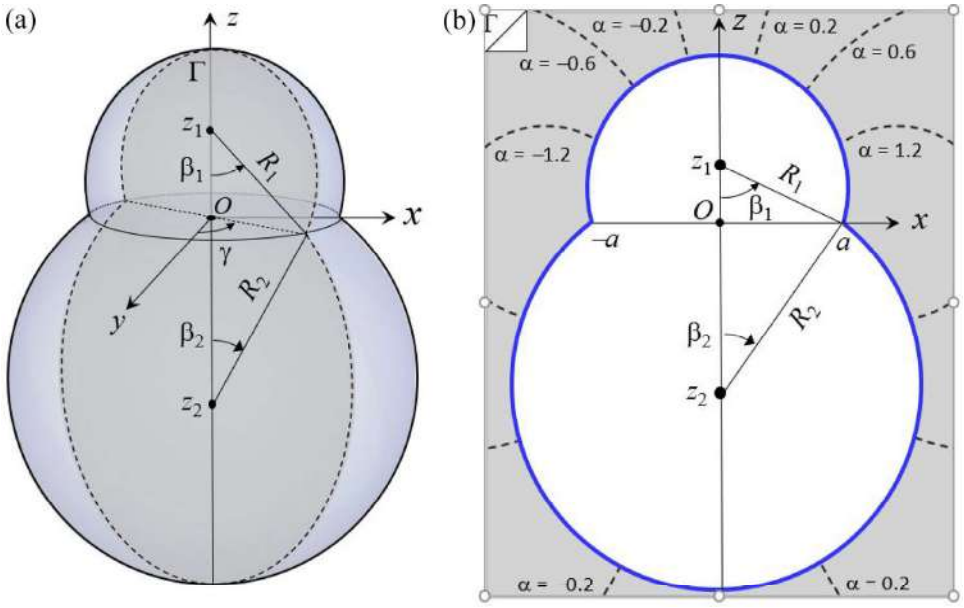

Figure 2. Sketch of the coalescing inhomogeneity referred to a toroidal coordinate system (a) and section of the coalescing inhomogeneity in the *xz* plane (b).

Two constant values of the bipolar coordinate β, namely, $\beta_1 > 0$ for the upper sphere and $\beta_2 < 0$ for the lower sphere, define the surfaces of the coalescing spheres. The surfaces of the spheres above and below the xy-plane read $x^2 + y^2 + (z - z_1)^2 = {R_1}^2$ and $x^2 + y^2 + (z + z_2)^2 = {R_2}^2$, respectively, with:

$$\beta_1 = \arccos(z_1/R_1), \qquad \beta_2 = -\arccos(z_2/R_2), \tag{2}$$

being $a = \sqrt{{R_1}^2 - z_1^2} = \sqrt{{R_2}^2 - z_2^2}$ in equation (1) the polar distance of the bipolar system.

The temperature distribution T under steady-state heat flux satisfies the Laplace equation:

$$\nabla^2 T = 0. \tag{3}$$

By introducing a new function [21]:

$$\Phi(\alpha, \beta) = \frac{T(\alpha, \beta)}{\sqrt{\cosh\alpha - \cos\beta}}, \tag{4}$$

condition (3) turns out to be:

$$\frac{\partial^2 \Phi}{\partial \alpha^2} + \coth\alpha \frac{\partial \Phi}{\partial \alpha} + \frac{\partial^2 \Phi}{\partial \beta^2} + \frac{\Phi}{4} = 0. \tag{5}$$

The Mehler–Fock transform [22,23] with respect to α:

$$\bar{\Phi}(\tau, \beta) = \tau \tanh \pi\tau \int_0^\infty \Phi(\alpha, \beta) P_{-1/2 + i\tau}(\cosh\alpha) \sinh\alpha \, d\alpha, \tag{6}$$

Please remove the white space in "$d\alpha$"

and its inverse:

$$\Phi(\alpha,\beta)=\int_0^{\infty}\bar{\Phi}(\tau,\beta)P_{-1/2+i\tau}(\cosh\alpha)d\alpha, \tag{7}$$

can be used to solve equation (5). Such a condition is reduced to the following ordinary differential equation (ODE):

$$\frac{\partial^2\bar{\Phi}}{\partial\beta^2}-\tau^2\bar{\Phi}=0, \tag{8}$$

which admits the general solution:

$$\bar{\Phi}(\tau,\beta)=A(\tau)\ \cosh\tau\beta+B(\tau)\ \sinh\tau\beta. \tag{9}$$

The heat flux is given by the isotropic Fourier law:

$$\boldsymbol{q}=-k\nabla T, \tag{10}$$

it is "(W m^{-1} K^{-1})"

where k is the heat conduction coefficient (W m^{-1} K^{-1}). Then, the boundary condition on the pore surface requires:

$$\boldsymbol{q}\cdot\boldsymbol{n}=0,\ \text{at}\ \beta=\beta_1>0\ \text{and}\ \beta=\beta_2<0, \tag{11}$$

where $\boldsymbol{n}$ is the outer unit normal on the double-sphere surface (Figure 2), coinciding with the unit vector $-\boldsymbol{e}_\beta$. Thus, from equation (11), the temperature field must satisfy the Neumann boundary condition at the surface of both the intersecting spheres as:

$$\frac{\partial T}{\partial\beta}=0,\ \text{at}\ \beta=\beta_1>0\ \text{and}\ \beta=\beta_2<0. \tag{12}$$

3. Applied flux along the z symmetry axis

Initially, we deal with the axisymmetric problem corresponding to a remote heat flux $\boldsymbol{q}_0=(0,\ 0,\ q_0)$ along the direction of the symmetry z-axis. We split the temperature field into the sum $T=T_0+T_1$, where T_0 is the fundamental contribution induced by the uniform heat flux in a homogeneous medium and T_1 denotes the corrective temperature field due to the presence of the coalesced spherical cavities. According to equation $(1)_3$, the fundamental contribution is given by:

$$T_0(\alpha,\ \beta)\ =-\frac{q_0}{k}\ \ z=\ -\frac{q_0\,a}{k}\frac{\sin\beta}{\cosh\alpha-\cos\beta}, \tag{13}$$

unless an arbitrary constant defining the reference temperature. The field T_0 is clearly harmonic and skew-symmetric with respect to β. Then, equation (3) implies that the field T_1 must also be harmonic. According to Morse and Feshbach [19], the corrective contribution turns out to be:

$$T_1(\alpha\ \beta)\ =\ \frac{q_0\,a}{k}\sqrt{\cosh\alpha-\cos\beta}\ \int_0^{\infty}P_{-1/2+i\tau}(\cosh\alpha)\ [u_1(\tau)\ \sinh\tau\beta+u_2(\tau)\ \cosh\tau\beta]\ d\tau, \tag{14}$$

"." instead of ","

The unknown functions $u_1(\tau)$, $u_2(\tau)$ must be found by imposing the boundary conditions (12) at $\beta=\beta_1,\beta_2$ (where $\beta_1>0$ and $\beta_2<0$), namely,

$$\frac{\sin\beta}{2\,(\cosh\alpha-\cos\beta)}\int_0^\infty [u_1(\tau)\sinh\tau\beta+u_2(\tau)\,\cosh\tau\beta]\;\;P_{-1/2+i\tau}(\cosh\alpha)\;d\tau+$$
$$\int_0^\infty \tau\;[u_2(\tau)\;\sinh\tau\beta+u_1(\tau)\;\cosh\tau\beta]\;P_{-1/2+i\tau}(\cosh\alpha)\;d\tau=\frac{\cosh\alpha\cos\beta-1}{(\cosh\alpha-\cos\beta)^{5/2}}. \tag{15}$$

Now, using the orthogonality relation [24]:

$$\int_0^\infty P_{-1/2+i\tau}(\cosh\alpha)\;P_{-1/2+i\eta}(\cosh\alpha)\;\sinh\alpha\;d\alpha=\frac{\delta(\tau-\eta)}{\tau\;\tanh\tau\pi}, \tag{16}$$

where δ is the Dirac delta, and the result (A.5) derived in the Appendix of Lanzoni et al. [16] one gets the following Fredholm integral equation of the second kind for the unknown functions u_1 and u_2 that must be imposed at $\beta=\beta_1,\beta_2$:

$$\frac{\sin\beta_k}{2}\int_0^\infty U_k(\tau,\eta)\;[u_1(\eta)\sinh\;\eta\beta_k+\;u_2(\eta)\;\cosh\;\eta\beta_k]\;d\eta+\frac{u_2(\tau)\;\sinh\;\tau\beta_k+\;u_1(\tau)\;\cosh\;\tau\beta_k}{\tanh\tau\pi}$$
$$=\frac{2\sqrt{2}}{3}\;\frac{\cot|\beta_k|\;\sinh\;\tau(\pi\;-|\beta_k|)-2\tau\;\cosh\;\tau(\pi\;-|\beta_k|)}{\sinh\;\tau\pi},\;\;k=\;1,\;2, \tag{17}$$

where the subkernel takes the form:

$$U_k(\tau,\eta)=\int_0^\infty \frac{P_{-1/2+i\tau}(\cosh\alpha)\;P_{-1/2+i\eta}(\cosh\alpha)}{\cosh\;\alpha-\cos\beta_k}\;\sinh\;\alpha\;d\alpha=\int_1^\infty \frac{P_{-0001/2+i\tau}(s)\;P_{-1/2+i\eta}(s)}{s-\cos\beta_k}\,ds. \tag{18}$$

leave "000"

[25, 28]

Note that $U_k(\tau,\eta)=U_k(\eta,\tau)$ [25] and the integral in equation (18) converges since $P_{-1/2+i\tau}(\cosh\alpha)$ decays as $e^{-\alpha/2}$ as α tends to infinity. The numerical calculation of the subkernel $U_k(\tau,\eta)$ is addressed as detailed in Appendix B in Lanzoni et al. [16].

In matrix form, the system (17) becomes:

$$\mathbf{A}(\tau)\;\mathbf{u}(\tau)+\int_0^\infty \mathbf{U}(\tau,\eta)\;\mathbf{B}(\eta)\;\mathbf{u}(\eta)\;d\eta=\mathbf{f}(\tau), \tag{19}$$

please insert some white spaces just after ","

where:

$$\mathbf{A}(\tau)=\frac{1}{\tanh\tau\pi}\begin{bmatrix}\cosh\;\tau\beta_1 & \sinh\;\tau\beta_1\\ \cosh\;\tau\beta_2 & \sinh\;\tau\beta_2\end{bmatrix},\mathbf{u}(\eta)=\begin{bmatrix}u_1(\eta)\\ u_2(\eta)\end{bmatrix},$$
$$\mathbf{U}(\tau,\eta)=\frac{1}{2}\begin{bmatrix}U_1(\tau,\eta)\;\sin\beta_1 & 0\\ 0 & U_2(\tau,\eta)\;\sin\beta_2\end{bmatrix},\mathbf{B}(\eta)=\begin{bmatrix}\sinh\eta_1 & \cosh\;\eta\beta_1\\ \sinh\;\eta\beta_2 & \cosh\;\eta\beta_2\end{bmatrix}, \tag{20}$$
$$\mathbf{f}(\tau)=\frac{2\sqrt{2}}{3\;\sinh\;\tau\pi}\begin{bmatrix}\cot|\beta_1|\;\sinh\;\tau(\pi\;-|\beta_1|)-2\tau\;\cosh\;\tau(\pi\;-|\beta_1|)\\ \cot|\beta_2|\;\sinh\;\tau(\pi\;-|\beta_2|)-2\tau\;\cosh\;\tau(\pi\;-|\beta_2|)\end{bmatrix}.$$

3.1. Numerical solution of the Fredholm integral equation

The numerical solution to the Fredholm integral equation (19) can be obtained using the Nyström method. We apply the Gauss–Laguerre quadrature rule for the semi-infinite interval to equation (23), obtaining (cf. Lanzoni et al. [16]):

$$\mathbf{A}(\tau)\ \mathbf{u}(\tau) + \sum_{j=1}^{n} w_j\ \mathbf{U}(\tau, \eta_j)\ \mathbf{B}(\eta_j)\ \mathbf{u}(\eta_j) = \mathbf{f}(\tau), \tag{21}$$

where η_j ($j = 1,\ 2,...,\ n$) are the Gauss–Laguerre quadrature points, coinciding with the roots of the Laguerre polynomial $L_n(\eta)$ of degree n, and:

$$w_j = \frac{\eta_j\ e^{\eta_j}}{(n+1)^2\ [L_{n+1}(\eta_j)]^2},\ \ (j = \ 1,\ 2, ..., n), \tag{22}$$

are the corresponding weights [26]. Equation (21) evaluated at the quadrature points then yields:

$$\mathbf{A}(\eta_i)\ \mathbf{u}(\eta_i) + \sum_{j=1}^{n} w_j\ \mathbf{U}(\eta_i, \eta_j)\ \mathbf{B}(\eta_j)\ \mathbf{u}(\eta_j) = \mathbf{f}(\eta_i), (i = \ 1,\ 2, ..., n). \tag{23}$$

This is a system of $2n$ linear algebraic equations in $2n$ scalar unknowns that can be solved for $\mathbf{u}(\eta_j)$ by standard techniques.

4. Applied flux orthogonal to the symmetry axis

In this section, we consider the non-axisymmetric problem corresponding to the heat flux directed along the y-axis orthogonal to the symmetry axis: $\boldsymbol{q}_0 = q_0\ \boldsymbol{e}_y$. In this case, the basic contribution T_0 reads:

$$T_0(\alpha, \beta) = \ -\frac{q_0}{k} y = \ -\frac{q_0 a}{k} \frac{\sinh\alpha\ \sin\gamma}{\cosh\alpha - \cos\beta}. \tag{24}$$

The field T_0 is harmonic and even with respect to β, and thus, the field T_1 is also harmonic and even with respect to β. The most general harmonic function in toroidal coordinates, which is even with respect to β and varies with $\sin\gamma$, has the following representation [19]:

$$T_1(\alpha, \beta)\ = \frac{q_0\, a}{k} \sqrt{\cosh\alpha - \cos\beta_k}\ \sin\gamma \int_0^{\infty} [u_1(\tau)\ \sinh\tau\beta_k + u_2(\tau)\ \cosh\tau\beta_k]\ P^{\,1}_{-1/2+i\tau}(\cosh\alpha)\ d\tau, \tag{25}$$

unless an arbitrary constant defining the reference temperature. In equation (25), $P^{\,1}_{-1/2+i\tau}$ is the first-order Legendre function of the first kind with complex index [20,27] which is vanishing at infinity. The unknown functions $u(\tau)$ must be found by imposing the boundary condition (12) at $\beta = \beta_1 > 0$ and $\beta = \beta_2 < 0$, namely, (with $k = 1, 2$):

$$\begin{aligned} &\frac{\sin\beta_k}{2\ (\cosh\alpha - \cos\beta_k)} \int_0^{\infty} [u_1(\tau)\ \sinh\tau\beta_k + u_2(\tau)\ \cosh\tau\beta_k]\ P^{1}_{-1/2+i\tau}(\cosh\alpha)\ d\tau + \\ &\int_0^{\infty} \tau\ [u_1(\tau)\cosh\tau\beta_k + u_2(\tau)\sinh\tau\beta_k]\ P^{1}_{-1/2+i\tau}(\cosh\alpha)\ \ d\tau = \ -\frac{\sinh\alpha \sin\beta_k}{(\cosh\alpha - \cos\beta_k)^{5/2}}. \end{aligned} \tag{26}$$

Based on the relation [24]:

is "," instead of "."

$$\int_0^\infty P^1_{-1/2+i\tau}(\cosh\alpha)\, P^1_{-1/2+i\eta}(\cosh\alpha)\, \sinh\alpha\, d\alpha = \frac{1+4\tau^2}{4\tau\, \tanh\tau\pi}\, \delta(\tau-\eta). \tag{27}$$

and the result (A.10) reported in Lanzoni et al. [16] one gets the following system of two Fredholm integral equations of the second kind for the unknown functions $u_1(\tau)$, $u_2(\tau)$ (with k = 1, 2):

"k" is slant: "*k*"

$$\begin{aligned} &\frac{1}{\tanh\tau\pi}\left(\tau^2+\frac{1}{4}\right)\left[u_1(\tau)\cosh\tau\beta_k + u_2(\tau)\sinh\tau\beta_k\right] + \\ &\frac{\sin\beta_k}{2}\int_0^\infty U_k(\tau,\eta)\left[u_1(\eta)\sinh\eta\beta_k + u_2(\eta)\cosh\eta\beta_k\right] d\eta = -\frac{\sqrt{2}}{3}(1+4\tau^2)\,\frac{\sinh\tau(\pi-\beta_k)}{\sinh\tau\pi}, \end{aligned} \tag{28}$$

being $U_k(\tau, \eta)$ the symmetric subkernel:

$$U_k(\tau,\eta) = \int_0^\infty \frac{P^1_{-1/2+i\tau}(\cosh\alpha)\, P^1_{-1/2+i\eta}(\cosh\alpha)}{\cosh\alpha-\cos\beta_k}\sinh\alpha\, d\alpha = \int_1^\infty \frac{P^1_{-1/2+i\tau}(s)\, P^1_{-1/2+i\eta}(s)}{s-\cos\beta_k}\, ds. \tag{29}$$

As before, one can write system (27) in matrix form as follows:

$$\mathbf{A}(\tau)\,\mathbf{u}(\tau) + \int_0^\infty \mathbf{U}(\tau,\eta)\,\mathbf{B}(\eta)\,\mathbf{u}(\eta)\, d\eta = \mathbf{f}(\tau), \tag{30}$$

please increase the white space after ","

where:

$$\begin{aligned} \mathbf{A}(\tau) &= \frac{1}{\tanh\tau\pi}\left(\tau^2+\frac{1}{4}\right)\begin{bmatrix}\cosh\tau\beta_1 & \sinh\tau\beta_1\\ \cosh\tau\beta_2 & \sinh\tau\beta_2\end{bmatrix}, \mathbf{u}(\eta) = \begin{bmatrix}u_1(\eta)\\ u_2(\eta)\end{bmatrix}, \\ \mathbf{U}(\tau,\eta) &= \frac{1}{2}\begin{bmatrix}U_1(\tau,\eta)\sin\beta_1 & 0\\ 0 & U_2(\tau,\eta)\sin\beta_2\end{bmatrix}, \mathbf{B}(\eta) = \begin{bmatrix}\sinh\eta\beta_1 & \cosh\eta\beta_1\\ \sinh\eta\beta_2 & \cosh\eta\beta_2\end{bmatrix}, \\ \mathbf{f}(\tau) &= -\frac{\sqrt{2}(1+4\tau^2)}{3\sinh\tau\pi}\begin{bmatrix}\sinh\tau(\pi-|\beta_1|)\\ \sinh\tau(\pi-|\beta_2|)\end{bmatrix}. \end{aligned} \tag{31}$$

System (30) is solved numerically using the Gauss–Laguerre quadrature, as done for system (21).

The dimensionless temperature field and the heat flow distributions for an inhomogeneity characterized by $\beta_1 = \pi/3$, $\beta_2 = -\pi/4$ are shown in Figure 3. In particular, Figure 3(a) and (c) deals with a heat flux acting along the symmetry axis, whereas Figure 3(b) and (d) concerns a heat flux transversal to the symmetry axis. Figure 3(c) and (d) highlights the fact that the obtained heat flux is tangent to the surface of the inhomogeneity, as required by the BCs (12). Note also from the maps displayed in Figure 3(a) and (b) that the heat flow field far from the inhomogeneity tends to assume a constant value, as required by the condition that the corrective contributions (14) and (25) must vanish at infinity to preserve the value of the applied heat flux.

5. Resistivity contribution tensor

The resistivity contribution tensor **R** for a pore or insulating inhomogeneity can be calculated combining equations (1.1) and (1.2):[AQ: 4]

[AQ4]: it is "... equations (10) and (11):"

$$\mathbf{R}\cdot\mathbf{q}_0 = \frac{1}{V_*}\int_S T\,\mathbf{n}\, dS, \tag{32}$$

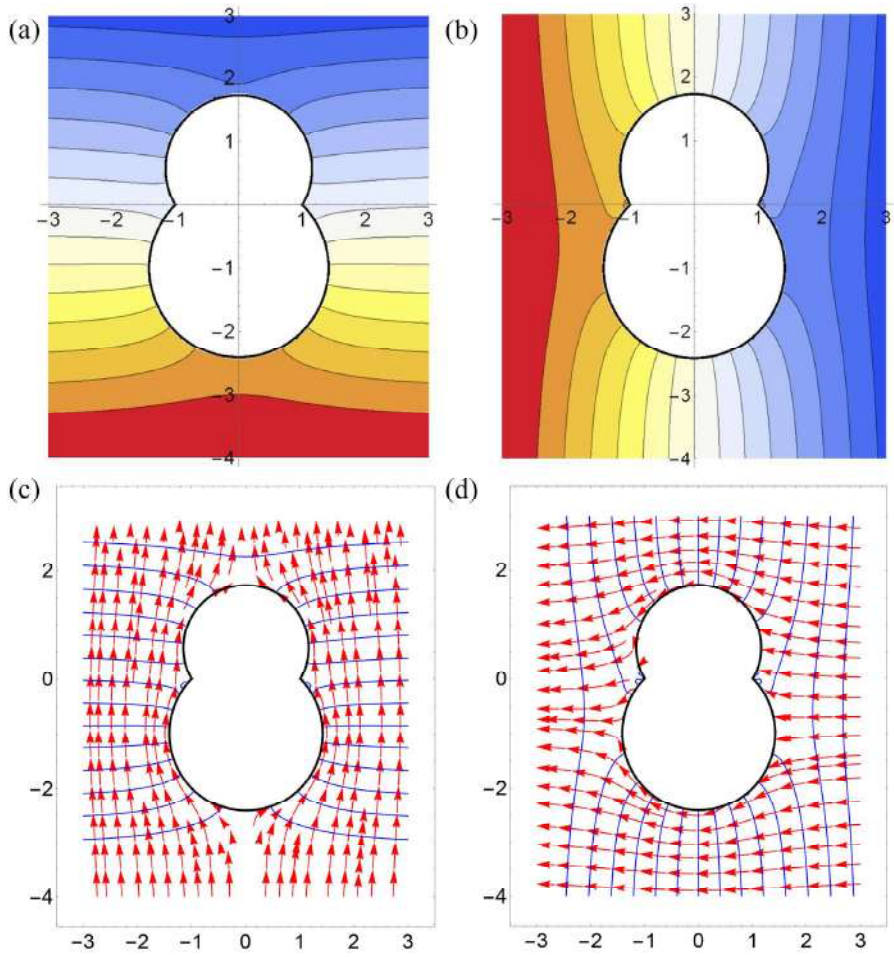

Figure 3. Temperature and heat flow fields for $\beta_1 = \pi/3$, $\beta_2 = -\pi/4$, for the remote heat flux $\mathbf{q}_0$ along the axial (a and c) and transversal (b and d) directions.

where $\mathbf{q}_0$ is the remote heat flux vector, and V_1 and S are the volume and surface of the pore, respectively. In particular, component R_{33} can be calculated using the axisymmetric solution given in section 3. The flux of temperature on the cavity surface $\beta = \beta_1, \beta_2$ is given by the surface integral:

$$\boldsymbol{\Phi} = \int_S T(\alpha,\ \beta_0)\,\mathbf{n}\,dA, \tag{33}$$

where $\mathbf{n} = -\mathbf{e}_\beta$ is the outer unit normal on the surface. Let $\mathbf{x}$ denote the position vector on the double-sphere surface, then using equation (1) one finds ($k = 1, 2$):

$$\begin{aligned}\mathbf{n}\,dA &= \frac{\partial \mathbf{x}}{\partial \alpha} \times \frac{\partial \mathbf{x}}{\partial \gamma}\,d\alpha\,d\gamma = \\ &= \{\sinh\alpha \sin\beta_k \cos\gamma,\ \sinh\alpha \sin\beta_k \sin\gamma,\ 1 - \cosh\alpha \cos\beta_k\}\,\frac{a^2 \sinh\alpha\ d\alpha\ d\gamma}{(\cosh\alpha - \cos\beta_k)^3},\end{aligned} \tag{34}$$

it is "." instead of ","

5.1. Heat flux along the symmetry axis

In the case of remote heat flux directed along the symmetry axis of the pore (z-axis), the sole non-vanishing component of the temperature flux vector (33) across the pore is ($k = 1, 2$):

$$\phi_z = 2\pi a^2 \sum_{k=1}^{2} \int_0^{\infty} \frac{1 - \cosh\alpha \cos\beta_k}{(\cosh\alpha - \cos\beta_k)^3} T(\alpha, \beta_k) \sinh\alpha \, d\alpha. \tag{35}$$

The substitution of the total temperature field $T = T_0 + T_1$ defined by equations (13) and (14) into equation (35) yields the total heat flux $\phi_z = \phi_z^{(0)} + \phi_z^{(1)}$, where ($k = 1, 2$):

$$\begin{aligned} \phi_z^{(0)} &= -2\pi a^3 \frac{q_0}{k} \sum_{k=1}^{2} \sin|\beta_k| \int_0^{\infty} \frac{1 - \cosh\alpha \cos\beta_k}{(\cosh\alpha - \cos\beta_k)^4} \sinh\alpha \, d\alpha \\ &= -\frac{q_0}{3k} \pi a^3 \sum_{k=1}^{2} \sin|\beta_k| \frac{2 - \cos\beta_k}{(1 - \cos\beta_k)^2}, \end{aligned} \tag{36}$$

and

$$\begin{aligned} \phi_z^{(1)} = \frac{q_0}{k} 2\pi a^3 \sum_{k=1}^{2} \sum_{j=1}^{n} w_j \left[u_1(\eta_j) \sinh\eta_j\beta_k + u_2(\eta_j) \cosh\eta_j\beta_k\right] \times \\ \int_0^{\infty} \frac{(1 - \cosh\alpha \cos\beta_k) \sinh\alpha}{(\cosh\alpha - \cos\beta_k)^{5/2}} P_{-1/2+i\eta_j}(\cosh\alpha) \, da. \end{aligned} \tag{37}$$

it is "$d\alpha$"

Using (A.5), equation (37) leads to the following expression ($k = 1, 2$):

$$\begin{aligned} \phi_z^{(1)} = -\frac{q_0}{k} \frac{4\sqrt{2}}{3} \pi a^3 \sum_{k=1}^{2} \operatorname{sign}(\beta_k) \sum_{j=1}^{n} w_j \left[u_1(\eta_j) \sinh\eta_j\beta_k + u_2(\eta_j) \cosh\eta_j\beta_k\right] \times \\ \frac{\cot|\beta_k| \sinh\eta_j(\pi - |\beta_k|) - 2\eta_j \cosh\eta_j(\pi - |\beta_k|)}{\sinh\eta_j\pi}. \end{aligned} \tag{38}$$

Then, the axial component of the resistivity contribution tensor is as follows:

$$R_{zz} = \frac{\phi_z}{V^* q_0}, \tag{39}$$

where:

$$V^* = \frac{\pi}{3} a^3 \sum_{k=1}^{2} \frac{2 + 3\cos\beta_k - \cos^3\beta_k}{\sin^3|\beta_k|}, \tag{40}$$

is the total volume of the inhomogeneity.

5.2. Heat flux orthogonal to the symmetry axis

In the case of remote heat flux orthogonal to the symmetry axis (namely, along y-axis), the sole non-vanishing component of the temperature flux vector (33) across the pore is ($k = 1, 2$):

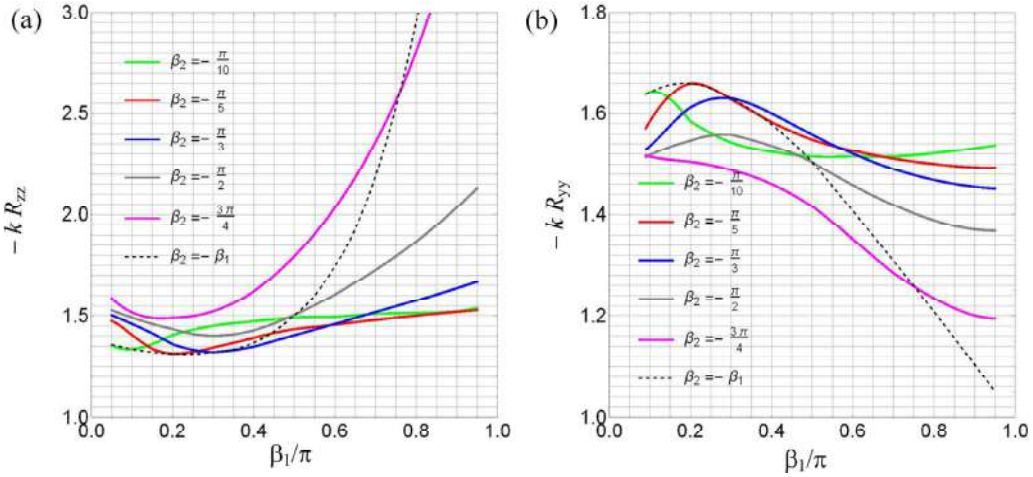

Figure 4. Normalized variations of the components of the resistivity contribution tensor for some selected values of β_2 varying β_1.

[AQ: 6]

[AQ6]: The caption becomes: "Normalized variations of the components R_{zz} (a) and R_{yy} (b) of the resistivity contribution tensor for some values of β_2 varying β_1.

$$\phi_y = a^2 \sum_{k=1}^{2} \sin\beta_k \int_0^{\infty} \frac{\sinh^2\alpha}{(\cosh\alpha - \cos\beta_k)^3}\, d\alpha \int_0^{2\pi} T(\alpha,\beta_k)\sin\gamma\, d\gamma. \tag{41}$$

The substitution of the total temperature field $T = T_0 + T_1$ defined by equations (24) and (25) into equation (41) yields the total heat flux $\phi_y = \phi_y^{(0)} + \phi_y^{(1)}$, where ($k = 1, 2$):

$$\phi_y^{(0)} = -\frac{q_0}{k}\pi a^3 \sum_{k=1}^{2} \sin\beta_k \int_0^{\infty} \frac{\sinh^3\alpha}{(\cosh\alpha - \cos\beta_k)^4}\, d\alpha = -\frac{q_0}{k}\pi a^3 \sum_{k=1}^{2} \frac{(2-\cos\beta_k)\,\sin\beta_k}{3(1-\cos\beta_k)^2}, \tag{42}$$

and

$$\phi_y^{(1)} = -\frac{q_0}{k}\pi a^3 \sum_{k=1}^{2} \sin\beta_k \sum_{j=1}^{n} w_j \left[u_1(\eta_j)\,\sinh\eta_j\beta_k + u_2(\eta_j)\,\cosh\eta_j\beta_k\right] \times \int_0^{\infty} \frac{\sinh^2\alpha}{(\cosh\alpha - \cos\beta_k)^{5/2}} P^1_{-1/2+i\eta_j}(\cosh\alpha)\, d\alpha. \tag{43}$$

Then, based on expressions (42) and (43), the transversal components of the resistivity contribution tensor can be assessed as follows:

$$R_{yy} = R_{xx} = \frac{\phi_y}{V^* q_0}, \tag{44}$$

where V^* is the volume of the inhomogeneity given in equation (40).

The variation of the dimensionless components of the resistivity contribution tensor is displayed in Figure 4(a) and (b) varying β_1 for some values of β_2. The dotted curve refers to the symmetric layout of two equal overlapping spheres reported in Lanzoni et al. [16] for which $\beta_1 = \beta_2$. As shown in those figures, the curves exhibit non-monotonic trends. In detail, for $\beta_1, \beta_2 < \pi/2$, i.e., when the inhomogeneity assumes a concave shape that can be inscribed into a prolate spheroid, the minima for the dimensionless component R_{zz} (and, correspondingly, the maxima for R_{yy} component) occur when $\beta_2 = -\beta_1$. This is confirmed by the fact that, for $\beta_1 < \pi/2$, the minima of the R_{zz} curves related to $\beta_2 < -\pi/2$ lie on the dotted curve that holds for $\beta_1 = -\beta_2$ (the black dashed curve in Figure 3(a) and (b)). Similarly, the

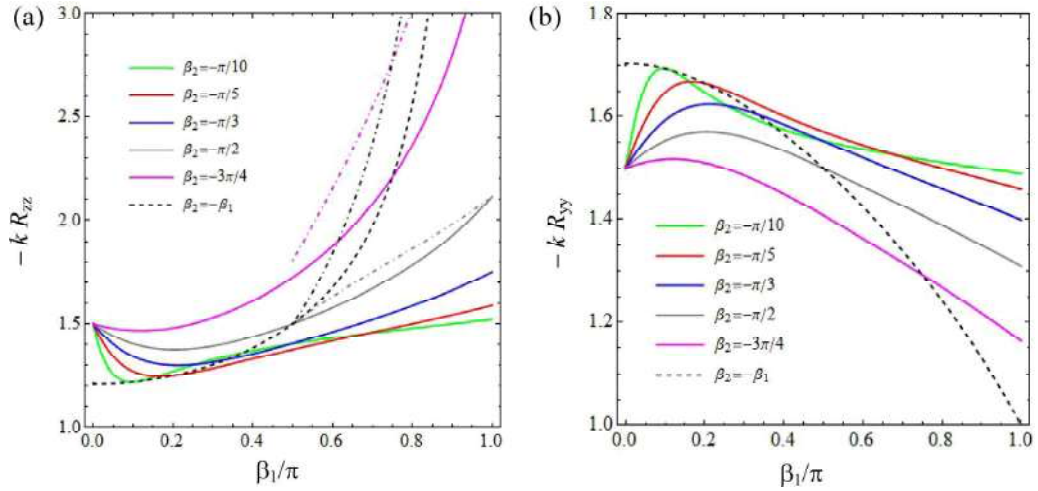

Figure 5. Normalized variations of the components of the resistivity contribution tensor of an equivalent insulating spheroid for some selected values of β_2 varying β_1. Solid and dash-dotted curves are obtained for approximating spheroids with aspect ratios given by equations (48) and (49), respectively[AQ: 7].

[AQ7]: The caption becomes: "Normalized variations of the components R_{zz} (a) and R_{yy} (b) of the resistivity contribution tensor of an.....

maxima of the R_{yy} curves lie on the dotted curve for $\beta_1 < \pi/2$. Conversely, for β_1 (or $|\beta_2|$) $\geqslant \pi/2$ (i.e., when one of the two spheres resembles a portion of an oblate spheroid), the extrema of both the components of the resistivity contribution tensor occur for $\beta_2 \neq -\beta_1$, i.e., for asymmetric dumbbell-shaped inhomogeneities. As an example, for $\beta_2 = -\pi/2$, the extrema of both R_{yy} and R_{zz} occur at $\beta_1 \cong 0.3\pi$. Note that, in general, when β_1 (or $-\beta_2$) $\geqslant \pi/2$, the stationary points of R_{yy} and R_{zz} do not occur for the same value of coordinate β_1. Note also that $-k\,R_{zz} = -k\,R_{yy} = 3/2$ when $\beta_1 - \beta_2 = \pi$, as expected for a spherical pore (see Lanzoni et al. [16]).[AQ: 5]

[AQ5]: sentence is ok.

5.3. Approximation by spheroidal inhomogeneities

Let us now compare the results obtained in equations (39) and (44) with those available for oblate and prolate spheroidal insulating inhomogeneities of the aspect ratio $\rho = b_s/a_s$ (see, for example, Kachanov and Sevostianov [13]), where a_s is the radius of the spheroid and b_s is the semi-axis of the spheroid along the z-axis, namely,

$$k\,R_{xx} = k\,R_{yy} = -\frac{1}{1-f_0}, \quad k\,R_{zz} = -\frac{1}{2f_0}, \tag{45}$$

where:

$$f_0 = \frac{\rho^2(1-g)}{2(\rho^2-1)}, g(\rho) = \begin{cases} \frac{1}{\rho\sqrt{1-\rho^2}}\arctan\frac{\sqrt{1-\rho^2}}{\rho}, & \text{oblate shape } (\rho<1) \\ \frac{1}{2\rho\sqrt{\rho^2-1}}\ln\frac{\rho+\sqrt{\rho^2-1}}{\rho-\sqrt{\rho^2-1}}, & \text{prolate shape } (\rho>1). \end{cases} \tag{46}$$

The components of the resistivity contribution tensor for an insulating inhomogeneity formed by two overlapping spheres of different size can be approximated with good accuracy by the corresponding components calculated for an insulating spheroid that has the same volume and the same height along the z-axis and, in turn, the following aspect ratio:

$$\rho = \frac{[R_1(1+\cos\beta_1)+R_2(1+\cos\beta_2)]^{3/2}}{\sqrt{2\left[R_1^3(2+3\cos\beta_1-\cos^3\beta_1)+R_2^3(2+3\cos\beta_2-\cos^3\beta_2)\right]}}, \tag{47}$$

namely,

$$\rho = \left(\frac{1+\cos\beta_1}{\sin\beta_1} - \frac{1+\cos\beta_2}{\sin\beta_2}\right)\sqrt{\frac{(1-\cos\beta_1)(1-\cos\beta_2)}{5+\cos(\beta_1-\beta_2)-3\cos\beta_1-3\cos\beta_2}}. \tag{48}$$

The normalized variations of the resistivity contribution tensor components provided by approximating spheroids for selected values of β_2 (the same values of Figure 3) varying β_1 are plotted in Figure 5. In general, these curves are close to those related to coalescing spheres in the neighboring of the points for which $\beta_1 - \beta_2 = \pi$, namely, when the inclusion resembles a sphere. Indeed, the approximation based on "equivalent" spheroids provides exact results for $\rho = 1$. In such a case, it is $g = 1$ and $f_0 = 1/3$, thus reproducing a spherical pore ($k\ R_{zz} = k\ R_{yy} = -3/2$). Except such specific layout, the best approximation is retrieved for R_{yy} when $\beta_2 = -3\pi/4$ for almost the entire range $0 < \beta_1 < \pi$. In such cases, the gap between the results provided by approximating spheroids and those related to the coalescing spheres is lower than 5% (see the pink curves in Figures 4(b) and 5(b)). When the inclusion resembles a dumbbell (i.e., for low values of both β_1 and β_2), the gap between the solution provided by the approximating spheroids and that of the intersecting spheres noteworthy increases. This result confirms previous analyses of literature about the rough predictions occurring when spheroids are adopted to approximate inclusions having concave surfaces (e.g., Kachanov and Sevostianov [13]). About R_{zz}, approximating spheroids lead to good predictions for $\beta_1 > \pi/2$ and $\beta_2 > -\pi/2$. In those cases, the maximum relative error between the approximated results and those related to coalescing spheres turns out to be 15%. When β_1 and $-\beta_2 \to \pi$, the inclusion resembles a penny-shaped crack. For such a situation, the procedure reported in sections 3 and 4 fails due to errors affecting the numerical solution of the Fredholm integral equations. Conversely, the approximation based on the "equivalent" spheroids provides $\rho \to 0$, $g \to \pi/(2\rho)$ and $f_0 \to 0$, thus giving $R_{xx} = R_{yy} = -1/k$ and $R_{zz} \to +\infty$.

When the inhomogeneity formed by the overlapping spheres assumes a lenticular shape (i.e., β_1 and $-\beta_2 > \pi/2$), the accuracy of the approximated results can be increased by keeping a spheroid having the same volume of the inhomogeneity and the radius equals to the polar distance (namely, $a_s = a$), thus giving the following aspect ratio:

$$\rho = \frac{1}{4}\left(\frac{2+3\cos\beta_1-\cos^3\beta_1}{\sin^3\beta_1} - \frac{2+3\cos\beta_2-\cos^3\beta_2}{\sin^3\beta_2}\right). \tag{49}$$

As an example, the dash-dotted curves in Figure 4(a) denote the R_{zz} component provided by approximating spheroids based on expression (49) in the range $\pi/2 < \beta_1$ for $\beta_2 = \pi/2$, $\beta_2 = 3\pi/4$, and $\beta_2 = -\beta_1$. For all these cases, the maximum relative gap among the exact results and the approximated, ones turns out to be 12%.

6. Conclusion

The problem of two non-conducting coalescing spheres of different size embedded in a 3D body subjected to an arbitrarily oriented and remotely applied steady-state heat flux is studied here. The temperature field is obtained as the sum of the fundamental solution for a homogeneous body plus a corrective term which allows satisfying the BCs at the surface of the inhomogeneity.

A system of two Fredholm integral equations is then obtained and solved based on the Nyström method, which is handled by performing the Gauss–Laguerre quadrature. The investigation is handled for the two cases of a heat flux directed along the symmetry axis and orthogonal to it. The obtained temperature fields are then used to assess the components of the second-rank resistivity contribution tensor. The study generalizes the results reported in Lanzoni et al. [16] for two non-conductive coalescing equal spheres. As shown in the present analysis, all the components of the resistivity contribution tensor exhibit a non-monotonic behavior with respect the size of the spheres expressed through β_1 and β_2 coordinates. In particular, for an inhomogeneity resembling a prolate spheroid, namely, for both β_1 and $\beta_2 < \pi/2$, R_{zz} shows a minimum and, at the same time, R_{yy} shows a maximum for $\beta_1 = \beta_2$. Conversely, when β_1 (or β_2) $\geqslant \pi/2$, the extrema for both R_{zz} and R_{yy} occur for β_2 (or β_1) $< \pi/2$, i.e., when the intersecting spheres have different size.

The approximation based on "equivalent" spheroids having the same height and volume of the coalescing spheres gives good predictions only for some geometrical layouts. In detail, R_{yy} component is reasonably well approximated by spheroids when $\beta_2 < -\pi/10$ and $\beta_1 > \pi/5$, whereas component R_{zz} is well approximated in the range $\pi/5 < \beta_1 < 0.7\pi$ for $-3\pi/4 < \beta_2$. Out of these intervals, the approximating spheroids generally lead to rough predictions. When the inhomogeneity assumes a lenticular shape, the accuracy provided by approximating spheroids to predict the R_{zz} component can be enhanced by keeping the radius of the spheroid equals to the polar distance and its volume as that of the inhomogeneity. However, it is worth noticing that the limiting cases of tangent spheres (β_1 and $\beta_2 \to 0$) and a penny-shaped crack (β_1 and $-\beta_2 \to \pi$) are not accurately recovered by the proposed formulation owing to numerical errors. A forthcoming work will be devoted to study the resistivity contribution tensor in the limiting case of two touching spheres.

Such results can be used as a benchmark to design composites materials containing inclusions of properly designed shapes to optimize thermal properties, electric conductivity, and so on. Further works will be devoted to the analysis of conductive intersecting spheres, thus involving challenging BCs.

Acknowledgements

L.L. gratefully acknowledges financial support from the Italian Ministry of Education, University and Research (MIUR) in the framework of the Project PRIN 2020 "*Opportunities and challenges of nanotechnology in advanced and green construction materials*" (code 2020EBLPLS; CUP E95F20002390001). E.R. gratefully acknowledges support from the POR FESR 2014–2020 project IMPReSA—"*Impiego di Materiali Plastici di Riciclo per malte e calcestruzzi Strutturali Alleggeriti*" (CUP. E81F18000310009).

Authors' note

This paper is dedicated to the memory of Igor Sevostianov.

Funding

The author(s) disclosed receipt of the following financial support for the research, authorship, and/or publication of this article:

ORCID iDs

Luca Lanzoni https://orcid.org/0000-0002-3513-0273
Enrico Radi https://orcid.org/0000-0002-7410-3008
Igor Sevostianov https://orcid.org/0000-0003-0809-3566

References

[AQ8]:All references have been correctly changed and properly quoted within the main text

[1] Park, J-G, Forster, JD, and Dufresne, ER. High-yield synthesis of monodisperse dumbbell-shaped polymer nanoparticles. *J Am Chem Soc* 2010; 132: 5960–5961[AQ: 8].
[2] Forster, JD, Park, J-G, Mittal, M, et al. Assembly of optical-scale dumbbells into dense photonic crystals. *ACS Nano* 2011; 5(8): 6695–6700.
[3] Sheu, HR, El-Aasser, MS, and Vanderhoff, JW. Phase separation in polystyrene latex interpenetrating polymer networks. *J Polym Sci A Polym Chem* 1990; 28: 629–651.
[4] Wang, C, Xu, C, Zeng, H, et al. Recent progress in syntheses and applications of dumbbell-like nanoparticles. *Adv Mater* 2009; 21: 3045–3052.
[5] Li, W, Ravaine, S, and Duguet, E. Clustering of asymmetric dumbbell-shaped silica/polystyrene nanoparticles by solvent-induced self-assembly. *J Colloid Interface Sci* 2020; 560: 639–648.
[6] Kim, H, Furst, E, Wang, Z, et al. Anisotropic phononic bandgaps in colloidal crystals of dumbbell-shaped nanoparticles. In: *APS march meeting 2021*, 15–19 March 2021, vol. 66. Bulletin of the American Physical Society, https://ui.adsabs.harvard.edu/abs/2021APS..MARE07013K/abstract
[7] Wang, Z, Kim, H, Secchi, M, et al. Quantization of acoustic modes in dumbbell nanoparticles. *Phys Rev Lett* 2022; 128(4): 048003.
[8] Chen, C-W, Hou, C-T, Li, C-C, et al. Large three-dimensional photonic crystals based on monocrystalline liquid crystal blue phases. *Nat Commun* 2017; 8: 727.
[9] Velikov, KP. Photonic crystals of shape-anisotropic colloidal particles. *Appl Phys Lett* 2002; 81: 838.

[10] Johnson, PM, van Kats, CM, and van Blaaderen, A. Synthesis of colloidal silica dumbbells. *Langmuir* 2005; 21: 11510–11517.
[11] Shen, H, Oppenheimer, SM, Dunand, DC, et al. Numerical modeling of pore size and distribution in foamed titanium. *Mech Mater* 2006; 38: 933–944.
[12] Manoylov, AV, Borodich, FM, and Evans, HP. Modelling of elastic properties of sintered porous materials. *Proc R Soc A* 2013; 469: 120689.
[13] Kachanov, M, and Sevostianov, I. *Micromechanics of materials, with applications*. Cham: Springer, 2018.
[14] Radi, E, and Sevostianov, I. Toroidal insulating inhomogeneity in an infinite space and related problems. *Proc R Soc A* 2016; 472: 20150781.
[15] Lanzoni, L, Radi, E, and Sevostianov, I. Effect of cylindrical fibers, with cross-sections formed by two circular arcs, on the overall conductivity of a composite. *Int J Solids Struct* 2018; 138: 264–276.
[16] Lanzoni, L, Radi, E, and Sevostianov, I. Effect of spherical pores coalescence on the overall conductivity of a material. *Mech Mater* 2020; 148: 103463.
[17] Krasnitckii, S, Trofimov, AL, Radi, E, et al. Effect of a rigid toroidal inhomogeneity on the elastic properties of a composite. *Math Mech Solids* 2019; 24: 1129–1146.
[18] Lanzoni, L, Radi, E, and Sevostianov, I. Effect of pair coalescence of circular pores on the overall elastic properties. *Int J Solids Struct* 2019; 172: 38–50.
[19] Morse, PM, and Feshbach, H. *Methods of theoretical physics, part 1*. New York: McGraw-Hill, 1953.
[20] Lebedev, NN, Skalskaya, IP, and Uflyand, YS. *Problems of mathematical physics*. Englewood Cliff, NJ: Prentice-Hall Inc., 1965.
[21] Liemert, A. Explicit solution for the electrostatic potential of the conducting double sphere. *J Appl Phys* 2014; 115: 164907.
[22] Ditkin, VA, and Prudnikov, AP. *Integral transforms and operational calculus*. Oxford: Pergamon Press, 1965.
[23] Sneddon, IN. *The use of integral transforms*. New York: McGraw-Hill, 1972.
[24] Gradshteyn, IS, and Ryzhik, IM. *Table of integrals, series, and products*. New York: Elsevier, 2007.
[25] Pitkonen, M. An explicit solution for the electric potential of the asymmetric dielectric double sphere. *J Phys D Appl Phys* 2007; 40: 1483–1488.
[26] Abramowitz, M, and Stegun, IA (eds). *Handbook of mathematical functions with formulas, graphs, and mathematical tables*. 9th printing. New York: Dover, 1972.
[27] Bateman, H, and Erdelyi, A. *Higher transcendental functions*, vol. 1. New York: McGraw-Hill, 1953.
[28] Felderhof, BU, and Palaniappan, D. Electrostatic capacitance of two unequal overlapping spheres and the rate of diffusion-controlled absorption. *J Appl Phys* 1999; 86: 6501–6506.[AQ: 9]

[AQ9]: ref [28] has to be cited together with [25] at p. 6, after eqn (18)